ACS APPLIED MATERIALS & INTERFACES

Research Article

www.acsami.org

Interfacial Morphology and Effects on Device Performance of Organic Bilayer Heterojunction Solar Cells

Michael Zawodzki,[†] Roland Resel,[†] Michele Sferrazza,[‡] Olivia Kettner,[†] and Bettina Friedel*[,†]

[†]Institute of Solid State Physics, Graz University of Technology, Graz, Styria 8010, Austria

[‡]Département de Physique, Université Libre de Bruxelles, 1050 Brussels, Belgium

Supporting Information

ABSTRACT: The effects of interface roughness between donor and acceptor in a bilayer heterojunction solar cell were investigated on a polymer−polymer system based on poly(3-hexylthiophene) (P3HT) and poly(dioctylfluorene-*alt*-benzothiadiazole) (F8BT). Both polymers are known to reorganize into semicrystalline structures when heated above their glass-transition temperature. Here, the bilayers were thermally annealed below glass transition of the bulk polymers (≈140 °C) at temperatures of 90, 100, and 110 °C for time periods from 2 min up to 250 min. No change of crystallinity could be observed at those temperatures. However, X-ray reflectivity and device characteristics reveal a coherent trend upon heat treatment. In X-ray reflectivity investigations, an increasing interface roughness between the two polymers is observed as a function of temperature and annealing time, up to a value of 1 nm. Simultaneously, according bilayer devices show an up to 80% increase of power conversion efficiency (PCE) for short annealing periods at any of the mentioned temperatures. Together, this is in agreement with the expectations for enlargement of the interfacial area. However, for longer annealing times, a decrease of PCE is observed, despite the ongoing increase of interface roughness. The onset of decreasing PCE shifts to shorter durations the higher the annealing temperature. Both, X-ray reflectivity and device characteristics display a significant change at temperatures below the glass transition temperatures of P3HT and F8BT.

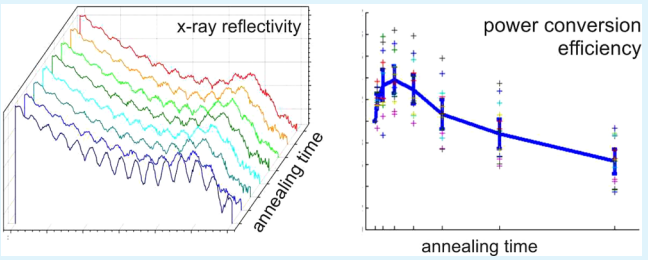

KEYWORDS: *all-polymer, solar cells, bilayer, floated, interface formation, low temperature annealing*

INTRODUCTION

Organic solar cells are a promising alternative to inorganic solar cells, because production costs can be reduced through different large area deposition techniques, like roll-to-roll.[1] Power conversion efficiencies around 10% are achieved right now with blends[2] or tandem cells.[3] Performance of an organic solar cell depends on several parameters; the most important ones are absorption of light to form an exciton, charge separation, charge carrier mobility, and charge collection at the electrodes. Absorption and mobility can be directly influenced by the choice of organic material, but the two other parameters are mainly determined by the device architecture itself. Charge collection can be improved with a better built-in potential or additional hole/electron conduction layers at the anode/cathode side. The charge separation is highly influenced by properties of an interfacial area between the donor and acceptor. This circumstance is related to the short lifetime of the Frenkel excitons, which corresponds to a short diffusion length of about 10 nm. This fact makes the distribution of donor and acceptor domains in the solar cell extremely vital. In the past, plenty of effort has been spent on the control of domain size and distribution in bulk-heterojunction blends by annealing of the organic semiconductors.[4,5] Thereby it is generally an accepted opinion that temperatures at or slightly above glass transition of the polymer are required to allow significant motion of polymer chain segments, allowing diffusion or reorientation.[6,7] Thereby it has been shown recently that the effective glass transition temperature (T_g) of polymer thin films can occasionally be slightly reduced compared to the bulk induced by free interface effects.[8]

The aim of this work is to determine the effects of low-temperature annealing (far below glass transition) on the interfacial morphology of a polymer−polymer bilayer and their consequences on the characteristics of an according organic solar cell. Investigated was a bilayer system of two semicrystalline polymers, the widely used P3HT as donor (D) and F8BT as acceptor (A). Various studies have already been performed on polymer bilayers to characterize the interfacial morphology,[9−13] thereby solely amorphous systems, annealing above glass transition or the effects of sequential spin-coating with orthogonal solvents have been investigated, but only seldomly these are directly compared to the performance of organic devices.[11,40] In this work, a sharp bilayer interface is generated by floating technique[39] and the interfacial morphology altered by thermal annealing below glass transition. This is characterized by X-ray reflectivity (XRR) and correlated with

Received: September 9, 2014
Accepted: July 7, 2015
Published: July 7, 2015

DOI: 10.1021/acsami.5b04972
ACS Appl. Mater. Interfaces 2015, 7, 16161−16168

the device physics of according solar cells. Please note that XRR probes the contrast of electron densities across the interface of different layer materials. Therefore, a distinction between (i) an interdiffusion of polymer chains from one layer into the other layer or (ii) an interface broadening of phase separated polymers cannot be made. As it is common practice for XRR, the interface morphology is given as an interface roughness reporting the average penetration of the two polymer layers into each other.

EXPERIMENTAL SECTION

Sample Preparation. The substrates (Spectrosil quartz glass, indium−tin-oxide (ITO) coated sodium silicate glass, and plain sodium silicate glass) were cleaned by sonication in methanol, acetone, and isopropyl alcohol (10 min each), followed by oxygen plasma etching (100 W, 10 min). The silicon substrates were treated in the same way except for methanol rinsing and plasma etching. The acceptor polymer poly[(9,9-di-*n*-octylfluorenyl-2,7-diyl)-*alt*-(benzo-[2,1,3]thiadiazol-4,8-diyl)] (F8BT) was provided by Cambridge Display Technology Ltd. with a molecular weight (M_W) of 150 kg mol^{-1}. Poly(3-hexylthiophene-2,5-diyl) (P3HT) was supplied by Rieke Metals Inc. with M_W of 70 kg mol^{-1} (regioregularity 93%, electronic grade). Chemical structures of the organic semiconductors are shown in Figure 1.

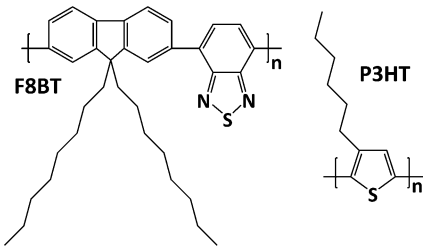

Figure 1. Chemical structures of F8BT (left) and P3HT (right).

All solutions of P3HT were prepared from anhydrous chlorobenzene (Sigma-Aldrich) at 100 °C for 20 min with concentrations of 8.5 g/L. F8BT was less soluble than P3HT and therefore stirred for 90 min at 100 °C with a concentration of 7.8 g/L. Films were deposited on Spectrosil quartz substrates for photophysical characterization and microscopy, on native silicon substrates for X-ray characterization, and on ITO glass for device fabrication. Single layer samples of P3HT or F8BT were spin-coated from hot solution directly onto the according substrate. For bilayer samples, P3HT was always spin-coated as the first layer. Subsequently, the F8BT as the second layer was first spin-coated onto a sodium glass substrate, lifted-off in demineralized water and floated onto the P3HT layer to avoid potential material intermixing, which can occur even with an orthogonal solvent.[11] A bilayer prepared with floating guarantees a sharp planar heterojunction interface and is ideal for the investigation concerning the interface morphology. Control samples of single layer F8BT by floating were also prepared to account for potential effects caused by the floating technique. Thickness of the layers was kept constant at 40 nm for P3HT and 60 nm for F8BT (facilitating XRR analysis). Photovoltaic devices were completed by evaporation of a 100 nm silver cathode and encapsulated (using an epoxy-glass combination) after preparation. To exclude additional effects from a second polymer/polymer interface, the commonly applied auxiliary layer of poly(3,4-ethylenedioxythiophene):polystyrenesulfonate (PEDOT:PSS) between ITO-substrate and the organic semiconductor layer was not applied. This approach was used to facilitate access to interface formation characteristics and has been used on a similar multilayer study in the past.[21]

Experimental Methods. The X-ray reflectivity (XRR) investigations were performed using an Empyrean PANalytical system in parallel beam geometry with a beam height of 100 μm and copper radiation Cu Kα. For all measurements the same setup was used, and just the scan parameters were changed. The bilayer samples were annealed with an Anton Paar DHS 900 heating stage under inert conditions.[14] The samples were heat treated in a temperature range from 90 °C−160 °C with annealing times from 2 min to 250 min. Reflectivity methods use specular conditions with means that the incident and diffracted angle of the beam enclose an equal angle relative to the substrate surface. Therefore, the reciprocal scattering vector q is perpendicular to the substrate surface, which means $q = q_z$. X'Pert Reflectivity software provided by PANalytical was used to fit the experimental data. Due to the appearance of a Bragg peak, the XRR data are only fitted up to 0.32 Å^{-1}. Grazing Incident X-ray Diffraction (GIXD) analysis was performed on a modified Bruker D8 Discover, using Cu Kα and an incident angle of α_i = 0.15°.[15] The lateral divergence was reduced to 0.35° with a Soller slit at the incident and diffracted side. The measured two-dimensional diffraction patterns are transferred into the reciprocal space using the in-plane scattering vector q_{xy} and the out-of-plane scattering vector q_z as coordinates. The integrated diffraction patterns (intensity versus q_{xy}) are obtained by integration of q_z in the region 0 Å^{-1} and 0.1 Å^{-1} at fixed values of q_{xy}. Atomic force microscopy (AFM) was performed using a Veeco Dimension 3100 AFM, operated in tapping mode. AFM images were recorded for single layers of P3HT, of F8BT, and of P3HT/F8BT bilayers, pristine, and after annealing at 100 °C for 5 min to investigate changing surface features. Surface roughness was deducted from AFM and was used to correlate with surface roughness of the films determined by XRR. Optical absorbance was measured on single layers and bilayer films deposited on Spectrosil quartz glass with a UV/vis spectrophotometer (Hewlett-Packard HP 8453). Photoluminescence (PL) spectra were measured in a nitrogen-purged integrating sphere under argon ion laser excitation at 515 nm at room temperature. Light was detected with an Oriel InstaSpec IV spectrograph. Photoluminescence quantum efficiencies (PLQE) were calculated for the P3HT emission, as described by de Mello et al.[16] Further, PL spectra were also recorded with a Shimadzu RF 5301PC spectrofluorometer under incoherent monochromatic light excitation at 400 nm (150 W xenon lamp) at room temperature. For photovoltaic device characterization, current−voltage characteristics were acquired under solar simulated conditions (intensity equivalent to 100 mW/cm^2, AM 1.5G) using a solar simulator light source (ABET Technologies 10500, specification ABB). Photovoltaic characterization was done for bilayer devices annealed at 90, 100, and 110 °C with an annealing time from 2 to 250 min. For every temperature/annealing step at least 12 devices were investigated.[22]

RESULTS

Interface Characterization. Figure 2 shows results of XRR for P3HT/F8BT bilayers, pristine, and after heat-treatment at temperatures of 140, 110, 100, and 90 °C. Thickness of the polymer single layers varied for P3HT from 39−43 nm and for F8BT from 61−64 nm, as extracted from XRR fits on single layers (compare the Supporting Information), which led to a predicted total bilayer thickness of 100 to 107 nm. This value was confirmed in XRR by the bilayers characteristic Kiessig-fringes below q_z = 0.20 Å^{-1} as seen in Figure 2, which correspond to the total thickness of the bilayer. Unfortunately, the lack of contrast in electron density between P3HT and F8BT of ρ_{P3HT} = 0.347 Å^{-3} and ρ_{F8BT} = 0.371 Å^{-3} result in a relatively low reflection coefficient at the P3HT/F8BT polymer interface; therefore, the X-ray beam was not able to differentiate the two layers from another at low q_z-values. However, above q_z = 0.20 Å^{-1} fringes from a thinner layer appear, which could be clearly assigned to the P3HT layer in-between the substrate and the F8BT layer. The emergence of P3HT-fringes at higher q_z-values is directly connected to the quality of the polymer interface and correlated to the roughness of the interface. This conclusion can be drawn from the fitting parameters obtained by modeling of the XRR data (compare Figure 3). Though the

DOI: 10.1021/acsami.5b04972
ACS Appl. Mater. Interfaces 2015, 7, 16161−16168

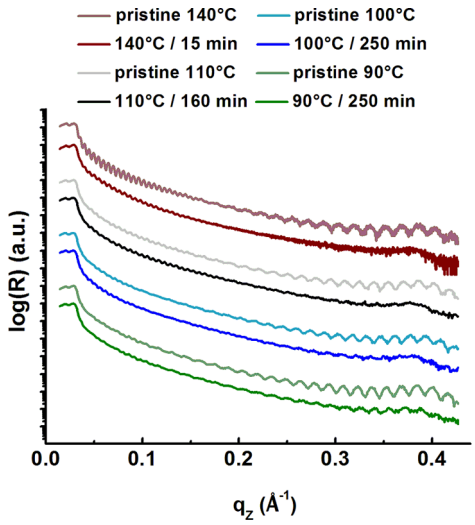

Figure 2. X-ray reflectivity measurements of P3HT/F8BT bilayers annealed at different temperatures and annealing times. For each sample the scans (in pairs) of the pristine (top curve) and the annealed (lower curve) film are shown.

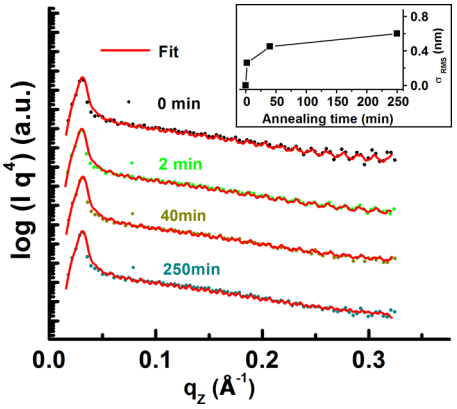

Figure 3. X-ray reflectivity curves of a P3HT/F8BT bilayer film annealed at a temperature of 100 °C. Starting from the pristine film (0 min), the annealing time was varied from 2 min over 40 to 250 min. The experimental data are plotted by symbols (due to clarity only every 20th experimental data point is plotted); the fitted curves are given by a red line. The inset gives the root-mean-square roughness (σ_{RMS}) of the polymer interface at different annealing times as obtained by the fit. The lines are guides for the eye.

used P3HT had relatively high molecular weight, lamellar ordering was not entirely suppressed, as indicated by an arising Bragg-peak at q_z = 0.38 Å^{-1}, seen more or less distinct in all films of Figure 2.

The fits for pristine as-made floated bilayers indeed indicate a sharp interface, with the determined interface roughness between P3HT and F8BT found negligible with $\sigma_{RMS} \approx 0$ nm. In the next step, the interface morphology was modified by thermal annealing. A polymer's glass transition temperature marks an important region of considerable change in its chain mobility. Therefore, a strong impact on the development of a polymer/polymer interface can be expected by annealing around this point. Glass transition is found for bulk-P3HT at $T_{g\text{-P3HT}}$ = 141 °C[17] and for bulk-F8BT depending on the molecular weight, between $T_{g\text{-F8BT}}$ = 125 °C (for M_W = 101 kg mol^{-1}) and $T_{g\text{-F8BT}}$ = 133 °C (for M_W = 220 kg mol^{-1}).[18] A heat treatment of a P3HT/F8BT bilayer at 140 °C for 15 min results already after this short period in a complete disappearance of the P3HT fringes (Figure 2). This indicates that at temperatures near T_g the interface roughness increases very fast. At lower temperatures this process is strongly delayed. At 110 °C different time scales of 2, 10, 30, 60, 100, and 160 min were applied, and a continuous decrease of the P3HT-fringes was observed only at longer annealing periods. In Figure 2 exemplarily the XRR-scan for 160 min annealing is shown, which demonstrates the strong reduction of the fringes, though they are still noticeable. When the temperature was reduced to 100 °C, the decay time of the P3HT fringes at high q_z-values became much longer. Only after applying an annealing period of 250 min, the fringes almost disappeared (Figure 2). For 90 °C, the decay of the P3HT-fringes was further suppressed, and so even after 250 min the P3HT-fringes were still clearly visible. To demonstrate the continuous decay of the P3HT-fringes with annealing time, Figure 3 shows XRR-scans and fits of bilayers in comparison, in pristine condition and after annealing at 100 °C for durations of 2, 20, and 250 min. The fits of these experimental data revealed continuous roughening of the polymer interface from almost zero to σ_{RMS} = 1 nm, as shown in the inset of Figure 3 (fit details are given in the Supporting Information). The observed increase of roughness at the P3HT/F8BT interface cannot be ascribed to effects of the glass transition temperature of the polymer bulk materials ($T_{g\text{-Bulk}}$) as the used temperatures were definitely below.

To determine if the obvious change of interfacial morphology correlates with a potential increase in crystallinity, GIXD measurements were performed on samples annealed at 100 °C for different periods between 2 and 250 min (compare the Supporting Information). Figure 4 exemplarily shows the

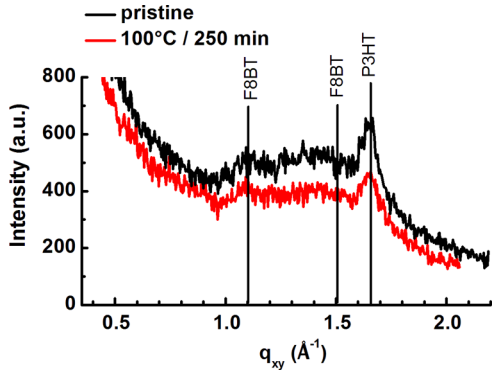

Figure 4. Integrated grazing incidence X-ray diffraction pattern of the pristine P3HT/F8BT bilayers and of the bilayer annealed at 100 °C for 250 min.

integrated diffraction patterns for a pristine and an annealed bilayer at 100 °C for 250 min in comparison. Both diffraction patterns show three distinct features. The first two subtle elevations around q_{xy} = 1.10 Å^{-1} and q_{xy} = 1.50 Å^{-1} are assigned to F8BT's characteristic side-by-side interchain distance (5.3 Å) and π-stacking (4.18 Å), respectively.[19] The weak and quite broad signal indicates little degree of order in the film. The third stronger peak is correlated to the interplanar distance between the π-stacked thiophene rings of P3HT at q_{xy} = 1.65 Å^{-1}.[20] It can be clearly seen that there is no significant change of the crystallinity of the bilayer. The small relative difference of both scans comes from a discrepancy of sample alignment and the use of different samples. Even after annealing close to $T_{g\text{-Bulk}}$ at 140 °C, the P3HT-peak does not change, neither in the

DOI: 10.1021/acsami.5b04972
ACS Appl. Mater. Interfaces 2015, 7, 16161−16168

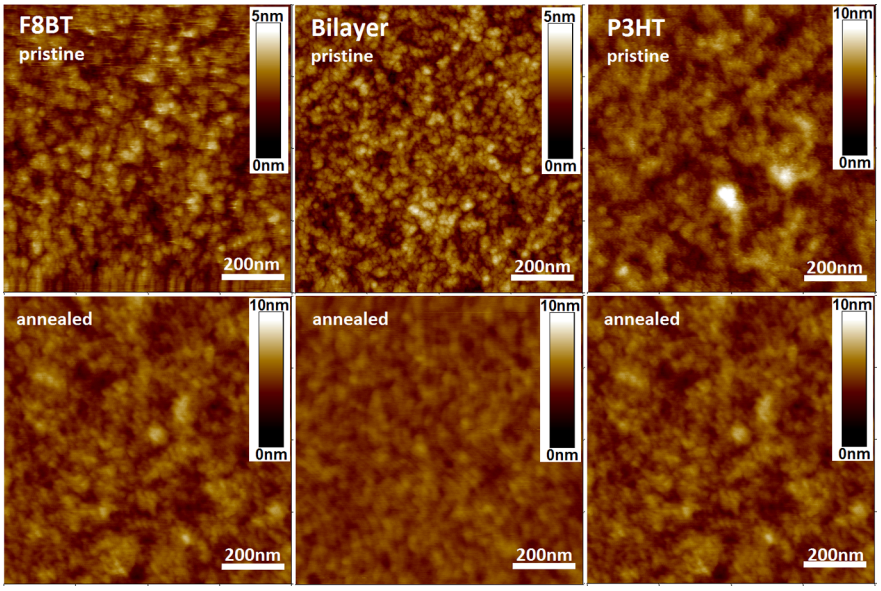

Figure 5. Atomic force microscopy height images of films of a single F8BT layer (left), of a P3HT/F8BT bilayer (middle, note: F8BT is the top-layer), and of a P3HT layer (right), pristine (top row) and after annealing at 100 °C for 5 min (bottom row).

GIXD-scans nor in specular scans at q_z = 0.38 Å^{-1} (Figure 2). It can be concluded that the crystallinity of the P3HT/F8BT bilayer does not change up to a temperature of 140 °C. However, experiments at 160 °C (annealed for 90 min) revealed a strong increase of crystallinity (not shown).

Figure 5 shows atomic force microscopy height images of a F8BT single layer, a P3HT/F8BT bilayer with F8BT on top, and a P3HT single layer; each surface is shown pristine (top) and after annealing at 100 °C for 5 min (bottom). Both, sole F8BT (Figure 5, left) and the bilayer (middle) show a considerable coarsening of the lateral feature size upon annealing from a few nanometers to up to 40 nm. At the same time, single layer P3HT (Figure 5, right) shows a reverse trend. These observations are reflected in surface roughness (σ_{RMS}) determined by AFM image analysis. This is showing a heat-induced increase from 0.38 to 0.56 nm in σ_{RMS} for F8BT single layers and 0.49 to 0.59 nm for bilayer samples. The same heat treatment on a P3HT single layer causes a decrease from 0.86 to 0.67 nm for σ_{RMS}. Despite the fact that different to XRR, AFM is a scanning-probe based technique with limited lateral resolution, the surface roughnesses of the pristine samples are in the same range as the corresponding fit parameters of the XRR data, with values of 0.39, 0.72, and 0.93 nm for F8BT, the bilayer, and P3HT, respectively.

Photophysics. The photoluminescence (PL) quenching can be a measure for the efficiency of exciton dissociation at the donor/acceptor interface, which is one essential step toward photocurrent generation. Exciton dissociation is strongly related to the D/A interface characteristics. Figure 6 shows emission spectra of P3HT/F8BT bilayer films, pristine and after annealing (100 °C, 5 min) upon excitation at 515 nm. This wavelength excites exclusively the donor P3HT phase, as visible from the absorbance spectrum of P3HT, additionally indicated in Figure 6. Accordingly, the emission of the pristine and annealed bilayer is dominated by PL of P3HT with a peak at 720 nm with vibrational shoulder at 690 nm, with only minor contribution from F8BT at the low wavelength side (note: F8BT absorption peaks at 460 nm, emission peaks at 540 nm, not shown). Thereby it can already be seen from the spectra

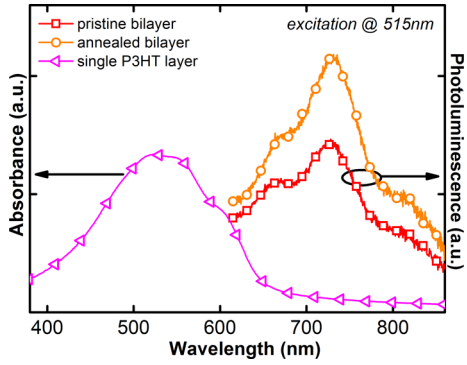

Figure 6. P3HT emission from pristine (red squares) and annealed (orange circles) bilayer films upon excitation at 515 nm. Absorption spectrum of pure P3HT (pink triangles) is shown for completeness. (Note: Symbols on the graphs are for indication).

that the PL intensities of the pristine and the annealed bilayer are quite different, with stronger emission obtained from the annealed bilayer. However, a clear quantitative result can only be delivered from measurement and calculation of photoluminescence quantum efficiency (PLQE). This has been determined for pure P3HT layers (pristine and annealed 100 °C, 5 min) and P3HT/F8BT bilayers (pristine and annealed 100 °C, 5 min). The PLQE for sole P3HT layers was found around 2.3%, independent of annealing. For the bilayers on the other hand, the PLQE was found to be only 1.4% for the pristine bilayer but almost 2.4% for the annealed bilayer. This means that in comparison the original P3HT emission is considerably quenched in the pristine bilayer but actually not noticeably in the annealed bilayer (note: even slightly higher than P3HT-only due to small F8BT contribution). As the PL of pure materials is not altered by annealing at that temperature, the obtained increase in PL from the pristine to the annealed blend can only be assigned to change at the polymer−polymer interface upon annealing. Typically, such decreased PL quenching is obtained when the donor/acceptor interfacial area is decreased, because less photogenerated excitons can

DOI: 10.1021/acsami.5b04972
ACS Appl. Mater. Interfaces 2015, 7, 16161−16168

reach a D/A interface to dissociate (within their small diffusion radius) and instead recombine radiatively.[29]

Photovoltaic Characteristics. Figure 7 shows photocurrent characteristics under simulated solar illumination

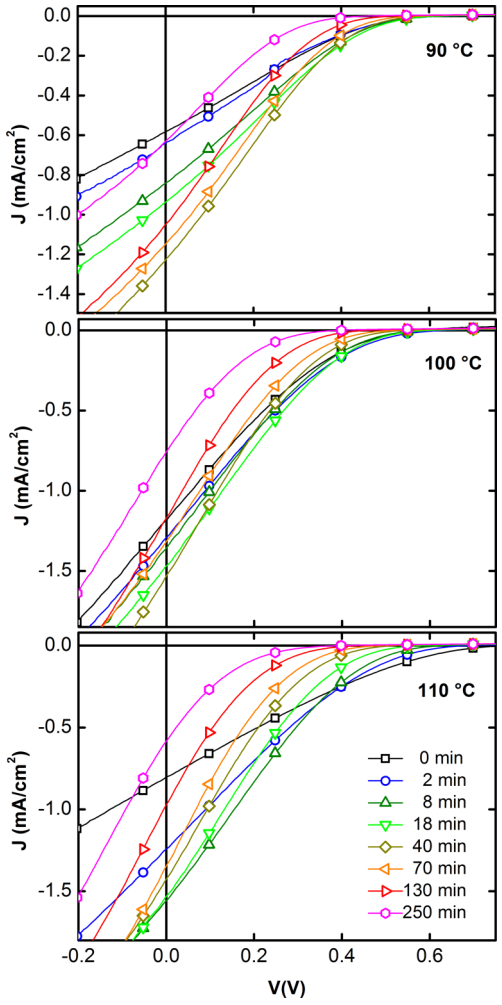

Figure 7. Photocurrent characteristics of P3HT/F8BT bilayer photovoltaic devices, as-deposited and after thermal treatment at 90, 100, or 110 °C for different annealing times. Symbols on the curves assign the corresponding plots.

(AM1.5G) of three representative P3HT/F8BT bilayer solar cells before and after annealing at temperatures of 90, 100, and 110 °C for time periods between 2 and 250 min. All IV curves show an S-shaped deterioration[22] in the fourth quadrant, accompanied by a low fill factor, independent of thermal treatment. It can be assumed that this is a result of the absence of the PEDOT:PSS interlayer, causing a hole-extraction barrier rising from energy level mismatch between ITO work function (∼−4.7 eV) and P3HT HOMO (∼−5.2 eV). For all temperatures and annealing times the fill factor of the devices is stable at 15 (±2)%, which suggests a thermally invariant interface formation between ITO and the spin-coated polymer. Strongly affected by thermal treatment of the bilayer are short circuit current (J_{SC}) and open circuit voltage (V_{OC}) of the devices. The J_{SC} for instance changes with annealing time, exhibiting a similar trend for all three temperatures. Thereby the J_{SC} starts lowest for the device with pristine bilayer and increases gradually with the duration of thermal treatment, until reaching a certain maximum in current. The required annealing time for reaching this maximum is shorter the higher the temperature, after 40 min for the 90 °C sample, between 18 and 40 min for 100 °C, and after only 8 min at 110 °C. For any of the annealing temperatures, exceeding the annealing time for reaching the maximum leads to a fast decrease in J_{SC} even below the value of the pristine sample. Another effect visible in the IV characteristics (Figure 7) is a significant drop of the V_{OC} upon thermal treatment, which does not entirely correlate with the observed J_{SC} trend. The highest V_{OC} of 1.1 V is close to the calculated possible maximum for this donor/acceptor combination ($HOMO_{P3HT} - LUMO_{F8BT} - 0.4$ eV ≈ 1.2 eV) but is observed only for pristine devices. Upon annealing, V_{OC} drops quickly with increasing annealing temperature and annealing time. At a temperature of 90 °C the V_{OC} decrease starts after 20 min, in the case of 100 °C after 8 min, and an immediate drop is observed at 110 °C. After the longest annealing duration of 250 min, the V_{OC} is reduced to 0.9 V for the 90 °C samples, 0.7 V for the 100 °C, and 0.6 V for the 110 °C devices. It should be noted that the graphs shown in Figure 7 are exemplarily from three devices, but representative, as statistical data of J_{SC} and V_{OC} confirm for a number of solar cells (given in the Supporting Information). The same phenomenon has been reported for solar cells with the P3HT:PC_{60}BM blend active layer, in space-application testing.[30] Thereby the devices were exposed to temperatures between 25 and 85 °C during operation, and also there parallel increase in J_{SC} and decrease in V_{OC} were observed with increasing temperature. The photocurrent increase was explained with promotion of thermally assisted hopping transport,[31] while degradation of the active layer was suggested as a potential reason for the decrease of V_{OC}.[32] As in this case the devices were tested at room temperature following thermal treatment, only factors which change the layer permanently can play a role.

The power conversion efficiency (PCE) is a product of fill factor, J_{SC} and V_{OC}, divided by incoming power. Figure 8 shows

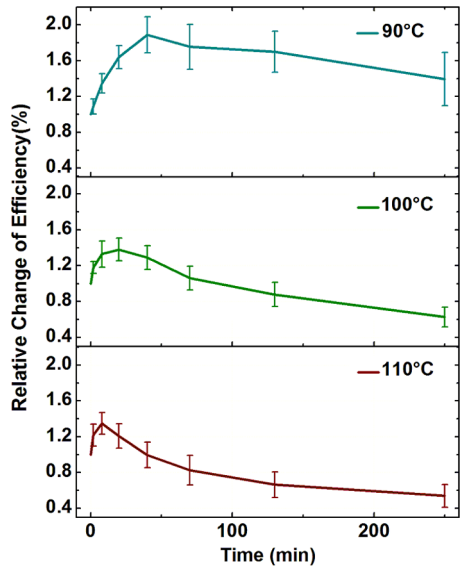

Figure 8. Evolution of power conversion efficiency (PCE) of P3HT/F8BT bilayer solar cells as a function of annealing temperature and annealing time. Shown is the PCE normalized to the initial value of the not-annealed device (0 min). The error bars give the variance from all measurements at particular annealing conditions.

DOI: 10.1021/acsami.5b04972
ACS Appl. Mater. Interfaces 2015, 7, 16161−16168

evolution of the device PCE upon annealing of the bilayer for the three temperatures 90, 100, and 110 °C with duration of the heat treatment. For better comparability the PCEs have been normalized to the initial efficiency value of a pristine bilayer device. For each of the annealing temperatures, again a similar trend is seen. The PCE starts from the value of the pristine bilayer and increases with duration of thermal treatment, up to a certain maximum point. The time after which this maximum is reached occurs after shorter durations the higher the temperature, which is after 40 min annealing at 90 °C, 20 min for 100 °C, and after only 8 min at 110 °C. Continued annealing beyond this duration causes in any case a reduction of PCE. Thereby at the highest temperature (110 °C) devices show the steepest drop in PCE, even below the value of the initial pristine bilayer device, while at 90 °C almost plateau-like behavior is observed, only decreasing over a long time. The observed trend in PCE is clearly a result of the superposition of the behavior of J_{SC} and V_{OC}.

DISCUSSION

Multiple studies reported interface roughening between two polymer layers by thermal annealing at glass transition temperature of the bulk material ($T_{g,Bulk}$) in the range of several nanometers.[9,11,13,27] Here, although a clear change of polymer morphology would not be expected by annealing below the polymers $T_{g,Bulk}$, X-ray reflectivity clearly revealed increasing interface roughness of the polymer−polymer interface between P3HT and F8BT. Its origin is either molecular interdiffusion generating a nanoscopic mixed phase or caused by microscopic interpenetration of the two phase-separated polymers. However, X-ray reflectivity is not able to distinguish between these two cases. The reason for such an effect occurring below $T_{g,Bulk}$ is not completely understood. A reduction of T_g in the order of 10 °C−30 °C was observed near free surfaces of polystyrene (PS) reaching tens of nanometers deep into the material.[23] For other polymers this effect was also observed but weakened by a factor of 3.[24] Different studies reported enhanced segmental mobility of polymers at free surfaces.[10,24−27] In the present case, reorganization at the film surface was confirmed with AFM imaging for single P3HT films (refinement) and single F8BT films (coarsening) after 100 °C annealing (see Figure 5). However, at the bilayer interface, being no free surface, such strong changes are not expected; but the X-ray reflectivity results in Figure 2 and Figure 3 show a clear increase of the interface roughness, if annealed below $T_{g\text{-}Bulk}$. Thereby the interface roughens faster (i.e., after shorter annealing time), the higher the temperature. Photophysical studies show clear quenching behavior of the P3HT photoluminescence by the presence of the F8BT acceptor layer in the pristine samples. However, thermal annealing of the bilayer causes increase in photoluminescence. As the single P3HT films' PL do not change with annealing, this must originate from diminished PL quenching at the D/A interface. Further, there are the device characteristics of the solar cells. The power conversion efficiency shows a particular trend, characterized by an initial increase with annealing time, followed by a drop. The maximum of the PCE thereby shifts to shorter annealing durations with increasing temperature (40 min @ 90 °C, 20 min @ 100 °C, and 8 min @ 110 °C). Thereby the PCE trend clearly reflects the superposition of photocurrent and open circuit voltage evolution. For the possible origin of the changes in J_{SC} and V_{OC} with thermal annealing below $T_{g\text{-}Bulk}$, the following effects could be responsible: (1) degradation of the active layer, (2) changes at the electrode interface (affected by contact resistance, interfacial area between active layer at the electrode), (3) de/increase in charge mobility by molecular reorganization, and (4) change of the D/A interfacial area.[30] There was no degradation of the active layers with ongoing annealing, as this would have shown as diminished PL also for sole P3HT films.[35] Variations at the contact (e.g., by dewetting of the polymer at the inorganic interface)[34] can be excluded since the observed fill factor is thermally invariant, which is a direct measure for the interfacial charge-transfer at the contact.[33] The charge carrier mobility of the individual polymer layers changes only modestly upon thermal annealing below $T_{g\text{-}Bulk}$ because substantial molecular reorganization is still suppressed.[28] Different studies have shown that charge mobility of F8BT does not change by annealing at 100 °C and even begins to decrease at $T_{g\text{-}Bulk}$.[11,18] For P3HT, annealing temperatures below $T_{g\text{-}Bulk}$, as in this case, change the charge carrier mobility by less than 1 order of magnitude.[28] Only if P3HT is annealed at/above $T_{g\text{-}Bulk}$, its hole-mobility increases considerably. This is also supported by XRD and XRR, as neither of them showed significant modifications in P3HT or F8BT at these temperatures. In conclusion, the evolution of the interface roughness must be directly and exclusively responsible for the observed development in J_{SC} and V_{OC} and PCE in consequence. It is suggested that at the onset of interface roughening of the bilayer there is indeed an increase of interfacial area between donor and acceptor, which has a direct beneficial impact on the amount of photocurrent generated, visible as increase of J_{SC}.[36] The V_{OC}, on the other hand, is only at maximum for the most sharp pristine interface, as the probability for flow of recombination currents (loss mechanism) is at minimum.[37] The ongoing increase of interface roughness beyond a certain point (max. J_{SC}) seems to create a morphology at the D/A interface, which no longer enhances photocurrent generation. Lowered J_{SC} and V_{OC} together with the decreased PL quenching indicates an increased rate of recombination. This usually occurs when the distance between a photogenerated exciton and the D/A interface (required for dissociation and generation of charge pairs) exceeds its diffusion length (in the range 10 nm).[38] With regard to the bilayer, this would imply that with ongoing interface roughening beyond the point of maximum device performance, too large inversions or even migrated separated droplets of one material within the other might have formed. However, as the highest observed interface roughness by XRR is 1 nm, this remains unclear.

CONCLUSIONS

The polymer bilayer of F8BT and P3HT was thermally annealed at temperatures below the glass transition temperature ($T_g \sim 140$ °C) of both polymers used, namely at 90, 100, 110, and 140 °C. No change of the crystallinity was observed in this temperature region. However, X-ray reflectivity showed a decrease of Kiessig fringes, which corresponds directly to the morphology at the bilayer interface. A continuous decrease of those fringes was observed for longer annealing periods (from 2 to 250 min) indicating a continuous increase of the interface roughness from almost zero to 1 nm. This effect of interface roughness appears at smaller annealing times when higher temperatures were applied. Also the photocurrent characteristics of the organic solar cells showed a serious change in the power conversion efficiency (PCE). In a first step an increase of up to 80% in PCE was measured, the reached maximum in PCE

DOI: 10.1021/acsami.5b04972
ACS Appl. Mater. Interfaces 2015, 7, 16161−16168

shifted from 40 min annealing at 90 °C, to 20 min annealing at 100 °C, to only 8 min annealing at 110 °C. After the observed maximum, an extension of the annealing time leads to a decrease of PCE, which is more pronounced at higher temperatures. Interestingly, the defined alteration of the device characteristics occurs at temperatures below the bulk-glass transition and therefore cannot be explained by changes of the charge carrier mobility but merely by the detected increase of the interface roughness.

■ ASSOCIATED CONTENT

Supporting Information

X-ray reflectivity investigations together with fit of the experimental data are given for the single layers of P3HT and F8BT as well as for the bilayer in the pristine state and annealed at 100 °C for 2, 20, and 120 min. All parameters of the fits are given. Grazing incidence X-ray diffraction of a pristine bilayer and of bilayers annealed at 100 °C between 2 and 250 min. Atomic force microscopy phase images of the single layers of P3HT and F8BT and of a bilayer in the pristine state and annealed at 100 °C for 5 min. Statistics in the device performance for devices annealed at 90, 100, and 110 °C for annealing times between 2 min up to 250 °C. The Supporting Information is available free of charge on the ACS Publications website at DOI: 10.1021/acsami.5b04972.

■ AUTHOR INFORMATION

Corresponding Author

*E-mail: bfriedel@tugraz.at.

Notes

The authors declare no competing financial interest.

■ ACKNOWLEDGMENTS

We are grateful to Cambridge Display Technology Ltd. (CDT) for the supply of materials and to Optoelectronics Group at the Cavendish Laboratory in Cambridge for access to photophysical characterization equipment. B.F. thanks the Austrian FWF for support through Grant no. P 26066-N20.

■ REFERENCES

(1) Krebs, F. C. All Solution Roll-to-Roll Processed Polymer Solar Cells Free from Indium-Tin-Oxide and Vacuum Coating Steps. *Org. Electron.* **2009**, *10*, 761−768.
(2) Scharber, M. C.; Mühlbacher, D.; Koppe, M.; Denk, P.; Waldauf, C.; Heeger, A. J.; Brabec, C. J. Design Rules for Donors in Bulk-Heterojunction Solar Cells — Towards 10% Energy-Conversion Efficiency. *Adv. Mater.* **2006**, *18*, 789−794.
(3) You, J.; Dou, L.; Yoshimura, K.; Kato, T.; Ohya, K.; Moriarty, T.; Emery, K.; Chen, C.-C.; Gao, J.; Li, G.; Yang, Y. A Polymer Tandem Solar Cell with 10.6% Power Conversion Efficiency. *Nat. Commun.* **2013**, *4*, 1446.
(4) Campoy-Quiles, M.; Ferenczi, T.; Agostinelli, T.; Etchegoin, P. G.; Kim, Y.; Anthopoulos, T. D.; Stavrinou, P. N.; Bradley; Donal, D. C.; Nelson, J. Morphology Evolution via Self-Organization and Lateral and Vertical Diffusion in Polymer: Fullerene Solar Cell Blends. *Nat. Mater.* **2008**, *7*, 158−164.
(5) Ruderer, M. A.; Guo, S.; Meier, R.; Chiang, H.-Y.; Körstgens, V.; Wiedersich, J.; Perlich, J.; Roth, S. V.; Müller-Buschbaum, P. Solvent-Induced Morphology in Polymer-Based Systems for Organic Photovoltaics. *Adv. Funct. Mater.* **2011**, *21*, 3382−3391.
(6) Brady, M. A.; Su, G. M.; Chabinyc, M. L. Recent Progress in the Morphology of Bulk Heterojunction Photovoltaics. *Soft Matter* **2011**, *7*, 11065−11077.
(7) Roland, C. M. Entropically Driven Miscibility in a Blend of High Molecular Weight Polymers. *Macromolecules* **1987**, *20*, 2557−2563.
(8) Bäumchen, O.; McGraw, J. D.; Forrest, J. A.; Dalnoki-Veress, K. Reduced Glass Transition Temperatures in Thin Polymer Films: Surface Effect or Artifact? *Phys. Rev. Lett.* **2012**, *109*, 055701.
(9) Higgins, A. M.; Martin, S. J.; Jukes, P. C.; Geoghegan, M.; Jones; Richard, A. L.; Langridge, S.; Cubitt, R.; Kirchmeyer, S.; Wehrum, A.; Grizzi, I. Interfacial Structure in Semiconducting Polymer Devices. *J. Mater. Chem.* **2003**, *13*, 2814−2818.
(10) Kraus, J.; Müller-Buschbaum, P.; Bucknall, D. G.; Stamm, M. J. Roughness Correlation and Interdiffusion in Thin Films of Polymer Chains. *J. Polym. Sci., Part B: Polym. Phys.* **1999**, *37*, 2862−2874.
(11) Yan, H.; Swaraj, S.; Wang, C.; Hwang, I.; Greenham, N. C.; Groves, C.; Ade, H.; McNeill, C. R. Influence of Annealing and Interfacial Roughness on the Performance of Bilayer Donor/Acceptor Polymer Photovoltaic Devices. *Adv. Funct. Mater.* **2010**, *20*, 4329−4337.
(12) Müller-Buschbaum, P.; Gutmann, J. S.; Kraus, J.; Walter, H.; Stamm, M. Suppression of Roughness Replication in Bilayer Films Prepared by Spin-Coating. *Macromolecules* **2000**, *33*, 569−576.
(13) Huettenbach, S.; Stamm, M.; Reiter, G.; Foster, M. The Interface Between Two Strongly Incompatible Polymers: Interfacial Broadening and Roughening near T_g. *Langmuir* **1991**, *7*, 2438−2442.
(14) Resel, R.; Tamas, E.; Sonderegger, B.; Hofbauer, P.; Keckes, J. A Heating Stage up to 1173 K for X-Ray Diffraction Studies in the Whole Orientation Space. *J. Appl. Crystallogr.* **2003**, *36*, 80−85.
(15) Neuschitzer, M.; Moser, A.; Neuhold, A.; Kraxner, J.; Stadlober, B.; Oehzelt, M.; Salzmann, I.; Resel, R.; Novák, J. Grazing-Incidence In-Plane X-Ray Diffraction on Ultra-Thin Organic Films Using Standard Laboratory Equipment. *J. Appl. Crystallogr.* **2012**, *45*, 367−370.
(16) de Mello, J. C.; Wittmann, H. F.; Friend, R. H. An Improved Experimental Determination of External Photoluminescence Quantum Efficiency. *Adv. Mater.* **1997**, *9*, 230−232.
(17) Friedel, B.; McNeill, C. R.; Greenham, N. C. Influence of Alkyl Side-Chain Length on the Performance of Poly(3-alkylthiophene)/Polyfluorene All-Polymer Solar Cells. *Chem. Mater.* **2010**, *22*, 3389−3398.
(18) Banach, M. J.; Friend, R. H.; Sirringhaus, H. Influence of the Molecular Weight on the Thermotropic Alignment of Thin Liquid Crystalline Polyfluorene Copolymer Films. *Macromolecules* **2003**, *36*, 2838−2844.
(19) Donley, C. L.; Zaumseil, J.; Andreasen, J. W.; Nielsen, M. M.; Sirringhaus, H.; Friend, R. H.; Kim, J.-S. Effects of Packing Structure on the Optoelectronic and Charge Transport Properties in Poly(9,9-di-n-octylfluorene-alt-benzothiadiazole). *J. Am. Chem. Soc.* **2005**, *127*, 12890−12899.
(20) Prosa, T. J.; Winokur, M. J.; Moulton, J.; Smith, P.; Heeger, A. J. X-Ray Structural Studies of Poly(3-alkylthiophenes): An Example of an Inverse Comb. *Macromolecules* **1992**, *25*, 4364−4372.
(21) Cataldo, S.; Sartorio, C.; Giannazzo, F.; Scandurra, A.; Pignataro, B. Self-Organization and Nanostructural Control in Thin Film Heterojunctions. *Nanoscale* **2014**, *6*, 3566−3575.
(22) Tress, W.; Corvers, S.; Leo, K.; Riede, M. Investigation of Driving Forces for Charge Extraction in Organic Solar Cells: Transient Photocurrent Measurements on Solar Cells Showing S-Shaped Current−Voltage Characteristics. *Adv. Energy Mater.* **2013**, *3*, 873−880.
(23) Ellison, C. J.; Torkelson, J. M. The Distribution of Glass-Transition Temperatures in Nanoscopically Confined Glass Formers. *Nat. Mater.* **2003**, *2*, 695−700.
(24) Roth, C. B.; McNerny, K. L.; Jager, W. F.; Torkelson, J. M. Eliminating the Enhanced Mobility at the Free Surface of Polystyrene: Fluorescence Studies of the Glass Transition Temperature in Thin Bilayer Films of Immiscible Polymers. *Macromolecules* **2007**, *40*, 2568−2574.
(25) Roth, C. B.; Dutcher, J. R. Glass Transition and Chain Mobility in Thin Polymer Films. *J. Electroanal. Chem.* **2005**, *584*, 13−22.

DOI: 10.1021/acsami.5b04972
ACS Appl. Mater. Interfaces 2015, 7, 16161−16168

(26) Kawana, S.; Jones, R. Character of the Glass Transition in Thin Supported Polymer Films. *Phys. Rev. E: Stat., Nonlinear, Soft Matter Phys.* **2001**, *63*, 021501.
(27) Mayes, A. M. Glass Transition of Amorphous Polymer Surfaces. *Macromolecules* **1994**, *27*, 3114−3115.
(28) Flesch, H.-G.; Resel, R.; McNeill, C. R. Charge Transport Properties and Microstructure of Polythiophene/Polyfluorene Blends. *Org. Electron.* **2009**, *10*, 1549−1555.
(29) McNeill, C. R. Morphology of All-Polymer Solar Cells. *Energy Environ. Sci.* **2012**, *5*, 5653−5667.
(30) Guo, S.; Brandt, C.; Andreev, T.; Metwalli, E.; Wang, W.; Perlich, J.; Müller-Buschbaum, P. First Step into Space: Performance and Morphological Evolution of P3HT:PCBM Bulk Heterojunction Solar Sells under AM0 Illumination. *ACS Appl. Mater. Interfaces* **2014**, *6*, 17902−17910.
(31) Mihailetchi, V. D.; van Duren, J.; Blom, P.; Hummelen, J. C.; Janssen, R.; Kroon, J. M.; Rispens, M. T.; Verhees, W.; Wienk, M. M. Electron Transport in a Methanofullerene. *Adv. Funct. Mater.* **2003**, *13*, 43−46.
(32) Peters, C. H.; Sachs-Quintana, I. T.; Mateker, W. R.; Heumueller, T.; Rivnay, J.; Noriega, R.; Beiley, Z. M.; Hoke, E. T.; Salleo, A.; McGehee, M. D. The Mechanism of Burn-in Loss in a High Efficiency Polymer Solar Cell. *Adv. Mater.* **2012**, *24*, 663−668.
(33) Grossiord, N.; Kroon, J. M.; Andriessen, R.; Blom, P. W. M. Degradation Mechanisms in Organic Photovoltaic Devices. *Org. Electron.* **2012**, *13*, 432−456.
(34) Müller-Buschbaum, P. Dewetting and Pattern Formation in Thin Polymer Films as Investigated in Real and Reciprocal Space. *J. Phys.: Condens. Matter* **2003**, *15*, R1549−R1582.
(35) Rösch, R.; Tanenbaum, D. M.; Jørgensen, M.; Seeland, M.; Bärenklau, M.; Hermenau, M.; Voroshazi, E.; Lloyd, M. T.; Galagan, Y.; Zimmermann, B.; Würfel, U.; Hösel, M.; Dam, H. F.; Gevorgyan, S. A.; Kudret, S.; Maes, W.; Lutsen, L.; Vanderzande, D.; Andriessen, R.; Teran-Escobar, G.; Lira-Cantu, M.; Rivaton, A.; Uzunoğlu, G. Y.; Germack, D.; Andreasen, B.; Madsen, M. V.; Norrman, K.; Hoppe, H.; Krebs, F. C. Investigation of the Degradation Mechanisms of a Variety of Organic Photovoltaic Devices by Combination of Imaging Techniques - the ISOS-3 Inter-Laboratory Collaboration. *Energy Environ. Sci.* **2012**, *5*, 6521−6540.
(36) Heremans, P.; Cheyns, D.; Rand, B. P. Strategies for Increasing the Efficiency of Heterojunction Organic Solar Cells: Material Selection and Device Architecture. *Acc. Chem. Res.* **2009**, *42*, 1740−1747.
(37) Tress, W.; Leo, K.; Riede, M. Optimum Mobility, Contact Properties, and Open-Circuit Voltage of Organic Solar Cells: A Drift-Diffusion Simulation Study. *Phys. Rev. B: Condens. Matter Mater. Phys.* **2012**, *85*, 155201.
(38) Halls, J. J. M.; Walsh, C. A.; Greenham, N. C.; Marseglia, E. A.; Friend, R. H.; Moratti, S. C.; Holmes, A. B. Efficient Photodiodes from Interpenetrating Polymer Networks. *Nature* **1995**, *376*, 498−500.
(39) Stein, N.; Korobko, R.; Yaffe, O.; Har Lavan, R.; Shpaisman, H.; Tirosh, E.; Vilan, A.; Cahen, D. Nondestructive Contact Deposition for Molecular Electronics: Si-Alkyl//Au Junctions. *J. Phys. Chem. C* **2010**, *114*, 12769−12776.
(40) Neuhold, A.; Brandner, H.; Ausserlechner, S. J.; Lorbek, S.; Neuschitzer, M.; Zojer, E.; Teichert, C.; Resel, R. X-ray Based Tools for the Investigation of Buried Interfaces in Organic Electronic Devices. *Org. Electron.* **2013**, *14*, 479−487.

DOI: 10.1021/acsami.5b04972
ACS Appl. Mater. Interfaces 2015, 7, 16161−16168